

# UV Continuum, Physical Conditions and Filling Factor in Active Galactic Nuclei

Lucimara P. Martins<sup>1</sup>

*Space Telescope Science Institute, 3700 San Martin Drive Baltimore, MD 21218*

`martins@stsci.edu`

Sueli M. Viegas & Ruth Gruenwald

*Instituto de Astronomia, Geofísica e Ciências Atmosféricas, São Paulo, Brazil*

## ABSTRACT

The narrow line region of active galaxies is formed by gas clouds surrounded by a diluted gas. Standard one-dimensional photoionization models are usually used to model this region in order to reproduce the observed emission lines. Since the narrow line region is not homogeneous, two major types of models are used: (a) those assuming a homogeneous gas distribution and a filling factor less than unity to mimic the presence of the emitting clouds; (b) those based on a composition of single-cloud models combined in order to obtain the observed spectra. The first method is largely used but may induce to misleading conclusions as shown in this paper. The second one is more appropriate, but requires a large number of observed lines in order to limit the number of single models used. After discussing the case of an extragalactic HII region, for which the ionizing radiation spectrum is better known, we show that 1-D models for the narrow line region with a filling factor less than unit do not properly mimic the clumpiness, but just simulates an overall lower density. Multi-cloud models lead to more reliable results. Both models are tested in this paper, using the emission-line spectra of two well-known Seyfert galaxies, NGC 4151 and NGC 1068. It is shown that ionizing radiation spectra with a blue bump cannot be excluded by multi-cloud models, although excluded by Alexander et al. (1999, 2000) using homogeneous models with a filling factor less than unity.

*Subject headings:* active galaxies; photoionization model; filling factor; multi-cloud models; ionizing radiation spectrum

---

<sup>1</sup>Instituto de Astronomia, Geofísica e Ciências Atmosféricas, São Paulo, Brazil

## 1. Introduction

The intrinsic spectral energy distribution (SED) of active galactic nuclei (AGN) extends from radio up to  $\gamma$  rays with observations available in a wide wavelength range. However, due to Galactic and intrinsic absorption, the SED above the Lyman limit cannot be observed. Since the main mechanism powering the emission-line spectrum of AGN is photoionization, it is important to know the shape of the UV radiation. As suggested by the observed continuum, it is usually assumed that the SED from ultraviolet to soft X-rays is basically a power law with at least two other components corresponding to the so-called “big blue bump”, usually represented by a blackbody radiation with temperature between  $1.5$  to  $3.0 \times 10^5$  K (see, for instance Oliva et al. 1994, Prieto & Viegas 2000), and to the soft X-ray excess, frequently described as a thermal component (see, for instance, Terashima et al. 2002). In addition, the SED is also important to test the emission by supermassive black holes and to discriminate among different models (Narayan, Kato & Homma 1997), as well as to help finding the signature of shocks in the narrow emission-line region (Contini, Viegas e Prieto 2002, and references therein).

Many observations of Seyfert galaxies point to the existence of three kinematically distinct emission regions: (a) an unresolved broad line region (BLR), with typical line widths of  $\geq 5000$  km s<sup>-1</sup>, densities above  $10^8$  cm<sup>-3</sup> and ionization parameter  $U \approx 0.03$ -1; (b) a narrow line region (NLR), with lower densities ( $\leq 10^7$  cm<sup>-3</sup>) and lower velocities ( $\leq 500$  km s<sup>-1</sup>) gas clouds with  $U$  in the range 0.03 to 0.1 embedded in a more diluted gas; (c) an extended emission-line region (EELR) with typical line widths of less than 50 km s<sup>-1</sup>, densities below  $10^3$  cm<sup>-3</sup>, and  $U$  smaller than 0.005 (Schulz and Komossa 1993).

The emission-line spectra of AGN show a rich variety of optical and UV lines, including those from highly ionized species (coronal lines). The observed line ratios point to photoionization as the dominant mechanism powering these objects. Recently, however, near infrared observations of narrow-line Sy 1 galaxies tend to favor shocks as the mechanism producing coronal lines (Rodriguez-Ardila et al. 2002). Nevertheless, photoionization being the main mechanism contributing to the emission-line spectra of AGN, photoionization models can be used to constrain the SED by fitting the observed lines.

Photoionization codes presently available were developed in the 70’s. They are one-dimensional (1-D) codes that usually assume a homogeneous gas distribution with a well-defined symmetry (plan-parallel or spherically symmetric). The standard input parameters are the shape and intensity of the ionizing radiation spectrum, the density of the gas, and the elemental abundances. Therefore, 1-D models are extremely limited to simulate clumpy regions like HII regions or the narrow line region of AGN.

In order to simulate an inhomogeneous region, two types of models are usually proposed: (a) those assuming a homogeneous distribution of gas and a filling factor less than unity (see, for instance Osterbrock 1989); (b) a multi-cloud model generated by a weighted average emission-line spectrum from single-cloud simulations (with  $\epsilon = 1$ ), as firstly proposed by Viegas-Aldrovandi & Gruenwald (1988), and more recently used by other authors (Baldwin et al. 1995, Binette, Wilson & Storchi-Bergmann 1996, Fergunson et al. 1997, Komossa & Shulz 1997, Kraemer & Crenshaw 2000). Multi-cloud models of the NLR, based on single-cloud models which take into account the coupled effect of photoionization and shocks, have also been used to analyze the NLR of AGN (Contini, Prieto & Viegas 1998a, 1998b, Contini & Viegas 2001, Contini et al. 2002).

The idea of a filling factor was first introduced by Osterbrock & Flatter (1959) in order to explain the radio brightness temperature of HII regions lower than expected, indicating that the gas has a clumpy distribution. The filling factor  $\epsilon$  is the fraction of the total volume occupied by the clumps or condensations. Since 1-D photoionization codes are unable to properly deal with an inhomogeneous gas distribution, the optical depth of each shell across the nebula is multiplied by the chosen filling factor (see, for instance, Osterbrock 1989). The net effect corresponds to a decrease of the average density, increasing the size of the ionized region, particularly the low ionization one, as it will be discussed below.

In the following, the expression ‘*model with a filling factor*’ refers to a model with a filling factor less than unity. Because of the increase of the low ionization zone relative to the high ionization zone, this kind of model tends to overestimate the low-ionization lines. Therefore, when simulating the NLR we must keep in mind this systematic effect and how it can affect the conclusions reached

A multi-cloud model offers a more realistic view of the NLR, as long as a proper choice of single-clouds (densities and ionization parameters) is achieved. Assuming that the chemical composition is the same, each group of single-clouds contributing to the emission-line spectrum is characterized by the density and ionization parameter (ratio of ionizing photons to gas density). The simulated emission-line spectrum corresponds to the weighted average of the line intensities coming from each group. The quality of the fit is related to the number of observed emission-lines. A better fit to the observed spectrum is obtained when a larger number of observed lines is available, allowing a fine tuning of the physical conditions producing the lines, leading to a better choice of the groups of single clouds.

Recently, NLR photoionization models have been used to constrain the shape of the spectral energy distribution of active nuclei (Oliva et al. 1994, Alexander et al. 1999 and 2000, Prieto & Viegas 2000). Here, our goal is to discuss the dependence of the SED on the type of model used to describe the NLR. Before analyzing the emission-line spectrum of two

Seyfert galaxies (NGC 4151 and NGC 1068), we discuss the filling factor problem related to photoionization models for extragalactic HII regions. For these objects the ionizing radiation spectrum is better known and the chemical composition obtained by empirical methods is reliable. Photoionization simulations of the NW knot of I Zw 18 provide a good example of the effect of a filling factor on the gas temperature and how models with a filling factor may induce to misleading results.

In §2, models for an extragalactic HII region are used to illustrate the effect of the filling factor, and a model for the NW knot of I Zw 18 is discussed. In §3, the observational data for NGC 1068 and NGC 4151 are presented, whereas photoionization models appear in §4. The concluding remarks are presented in §5.

## 2. Filling Factor Models

The effect of  $\epsilon < 1$  in 1-D models is to increase the size of the low-ionization zone, consequently increasing the ionized region and reducing the average temperature of the ionized gas. Models with  $\epsilon = 1$  should provide a higher average gas temperature, increasing the calculated [O III] line ratio. In order to illustrate the effect of a filling factor less than unit, the results of HII region models with  $\epsilon \leq 1$ , obtained by the 1-D code Aangaba (Gruenwald & Viegas 1992), are discussed.

We adopt the ionizing radiation of a zero age stellar cluster from Cid-Fernandes et al. (1992) shown in Figure 1 (top panel), with a number of ionizing photons  $Q_H = 10^{51} \text{ s}^{-1}$ , a uniform distribution of the gas with hydrogen density equal to  $100 \text{ cm}^{-3}$ , and chemical abundances of I Zw 18 (Izotov & Thuan 1998). The results obtained for the outer radius of the HII region, as well as the average temperature  $T_{OIII}$ , as a function of  $\epsilon$ , are shown in Figure 1 (middle panel), while the ionic fractions of  $O^0$ ,  $O^+$  and  $O^{++}$  appear in Figure 1 (bottom panel). As expected, the outer radius,  $O^0$  and  $O^+$  increase with decreasing  $\epsilon$ , while  $T_{OIII}$  and  $O^{++}$  decrease, corresponding to the expansion of the low-ionization zone for smaller values of  $\epsilon$ .

The shape of the ionizing radiation is another factor defining the relative size of the high-ionization to the low-ionization zone. To exemplify this point the zero age stellar cluster continuum spectrum was modified between 1 Ryd and 4 Ryd (Fig. 1, top panel) and the results are also shown in Figure 1 (middle and bottom panels). The filling factor effect is similar for the two types of ionizing spectra. However, the ionic fractions of  $O^+$  and  $O^{++}$  are larger while the  $O^0$  fraction is lower when the spectrum has less photons near the Lyman limit. Notice that, in this case,  $O^{++}/O$  increases by a larger amount. Ions of other elements

follow the same behavior. Therefore, the increase of the low-ionization zone due to a filling factor less than unity, leading to stronger low-ionization emission-lines, can be compensated by adopting an ionizing radiation with less photons near the Lyman limit.

## 2.1. The Star Forming Galaxy I Zw 18

Recently, 1-D photoionization models for the NW knot of I Zw 18, a metal poor extragalactic HII region, have been used by Stasinska & Schaerer (1999, hereafter SS99) to analyze its emission-line spectrum. They concluded that in addition to photoionization, another heating mechanism is necessary in order to explain all observed features, i. e., the size of the ionized region, the  $H\beta$  luminosity and the emission-line ratios of the more significant lines.

In order to model the NW knot, SS99 adopted a homogeneous gas distribution with density equal to  $100 \text{ cm}^{-3}$ , derived from the observed [S II] line ratio, as well as the chemical abundances obtained by Izotov & Thuan (1998). The best fit model should reproduce the significant emission-line ratios, the  $H\beta$  luminosity, as well as the size of the ionized region. Adjusting the total initial mass of the stellar cluster in order to reproduce the luminosity, the authors show that a homogeneous model may explain some of the line ratios, but the calculated size of the ionized region is too small unless a filling factor of the order of 0.01 is adopted. Their best fit model corresponds to an homogeneous model with this filling factor, combined with condensations simulated by higher density models. All the observed features are explained except for the observed [O III]  $\lambda 4363/5007$  line ratio, the calculated ratio being too low. Because this ratio is a temperature indicator, the authors concluded that an additional heating source must be present in the NW knot and suggested the possible presence of shocks.

Following Viegas, Contini & Contini (1999), shocks must be contributing to the observed emission-lines of starburst galaxies depending on the evolutionary phase of the stellar cluster and could be identified as an additional heating mechanism. However, I Zw 18 is a metal poor extragalactic HII galaxy where the shock contribution to the physical conditions is negligible. Such effects could only be significant in evolved star forming regions. In order to analyze the apparent discrepancy between the need for an additional heating source and the characteristics of I Zw 18, the SS99 model assumptions have been reviewed (see Viegas 2002 for more details), using the code Aangaba.

Following SS99,  $\epsilon < 1$  is necessary in order to match the size of the ionized region. However, a model with  $\epsilon = 1$  and a lower density could reproduce it. Notice that a density

of about  $30 \text{ cm}^{-3}$  is also in agreement with the observed [S II] ratio. In fact, Viegas (2002) showed that a uniform density model for a spherical region with  $n = 30 \text{ cm}^{-3}$  and filling factor equal to unit, photoionized by a 5.4 Myr stellar cluster, reproduces the size of the NW knot and the  $H\beta$  luminosity, although some of the observed line ratios are not explained. The same kind of discrepancy between observational and theoretical line ratios was reported by SS99 concerning the homogenous model. These authors suggested the presence of condensations to improve the fitting. In fact, an inhomogeneous gas distribution is suggested by the HST image of I Zw 18. Two other models with a higher density ( $10^4 \text{ cm}^{-3}$ ), mimicking possible condensations, are also presented by Viegas (2002), showing that the emission-line intensities, the  $H\beta$  luminosity, as well as the size of the emission region, are well reproduced with no need of an additional heating mechanism.

No specific combination of dense and dilute gas is provided by SS99, but they show that the presence of condensations improves the results for the [O I] emission line, which was too low in the homogeneous model. The results obtained by Viegas (2002) with dense gas ( $10^4 \text{ cm}^{-3}$ ) at different distances from the stellar cluster indicated that the best choice is a set of condensations located in the outer zone of the ionized region. Notice that a large fraction of  $H\beta$  is emitted in the inner zone. Taking these facts into account, an example of a composite model for the NW knot of I Zw 18 is presented in Figure 2, where the results for a dilute uniform gas ( $30 \text{ cm}^{-3}$ , filled circle) and a denser gas ( $10^4 \text{ cm}^{-3}$ , filled square) are combined (circle) assuming that 60% of  $H\beta$  comes from the low density gas and the remaining 40% from condensations. This model provides a very good fit of the line ratios, as well as of the size of the ionized region and of the average  $T_{OIII}$ . The results presented in Fig. 2 make clear the potential of multi-cloud models to reproduce inhomogeneous regions without the problems associated with models with a filling factor less than unity. It is not our intention to claim that this is the best model for the NW knot of I Zw 18, but just to exemplify how an artificial problem created by models with filling factor can be solved by composite models. Notice, however, that a reliable composite model requires the fitting of large number of observed lines, not only the most significant ones.

In brief, the adoption of a filling factor led to a “heating problem” and, consequently, to the suggestion of the presence of shocks, whereas a composite model, built from single-cloud models with different densities and  $\epsilon = 1$ , explains all the observable features without requiring an additional heating mechanism, in agreement with the conclusions from Viegas et al. (1999). In this case, the misleading effect of a filling factor less than unity – *artificially increasing the low-ionization zone of the cloud and decreasing the average temperature of the gas* – could be easily identified because the ionizing radiation spectrum is well known. However, for the NLR of AGN the “filling factor effect” could influence the choice of the shape of the unknown UV ionizing radiation spectrum inferred from the models, as discussed

below for two Seyfert galaxies, NGC 1068 and NGC 4151.

### 3. NGC 4151 and NGC 1068 Observational Data

NGC 4151 is a spiral galaxy, almost face-on, with  $z = 0.0033$  and magnitude  $m_V = 11.5$ . Its continuum spectrum is dominated by a non-stellar component (Kaspi et al. 1996) which is extremely variable, as are the broad emission lines. This galaxy is usually given as an example of a classic Seyfert galaxy, but it shows a variety of physical properties of different AGN classes. It could then be more complex than the average Seyfert galaxies. Originally classified as an intermediate Sy 1.5 galaxy (Osterbrock & Koski 1976), it presented the characteristics of a Sy 2 during its extremely low state in 1984 (Penson & Perez 1984). Currently NGC 4151 is classified as a Sy 1 galaxy.

NGC 1068 is one of the brightest and closest known Sy 2 galaxies. It is also the archetypal “hidden Seyfert 1” galaxy, following the unified model for active galactic nuclei (Antonucci & Miller 1985, Antonucci 1993). The narrow-line region is approximately co-spatial with a linear radio source with two lobes (Wilson & Ulvestad 1983). Most of the NLR and extended emission line region are likely powered by photoionization by a central source (Marconi et al. 1996). Moreover, high-resolution observations suggest kinematic disturbance and possibly shock excitation of regions close to the radio outflow (e.g. Axon et al. 1998).

Both objects have already been modeled by Alexander et al. (1999) and Alexander et al. (2000) (hereafter A99 and A00, respectively), using photoionization models with a filling factor. These authors used the observed emission-lines to constrain the ionizing continuum spectral shape, in particular to discuss the presence of a blue bump. On the other hand, two-component photoionization models, with a broken power law, have been used by Kraemer & Crenshaw (2000) to reproduce the emission-line spectra of NGC 1068. Multi-cloud models, which take into account the coupled effect of photoionization by a power-law ionizing radiation and shocks, are also discussed by Contini et al. (2002) for NGC 4151.

In order to discuss the filling factor effect on the inferred SED of the ionizing radiation, NLR of these two AGN are modeled in this work. We will adopt the list of observed emission-lines of NGC 4151 and NGC 1068 from A99 and A00, respectively. They provide a list of emission-lines carefully selected according to the following criteria: (a) only lines that are primarily formed by photoionization due to an UV – soft X-ray continuum from a central source are included; (b) all lines emitted from ions with ionization potential less than 13.6

eV are excluded, since these ions can be easily ionized by other processes; (c) only lines with reliable flux measurements are included, requiring that the line measurements are not too inconsistent with the large SWS and LWS (ISO Short- and Long-Wavelength Spectrometer, respectively) apertures; and finally, (d) they excluded the [FeX] 6734 Å and [FeXI] 7892 Å coronal lines, because the collision strength values are highly uncertain. Whenever more than one measurement for these lines exists, they quote the average flux and use rms scatter as an error estimate.

Notice that A99 compare the emission-line absolute fluxes of NGC 4151 to the model results, instead of the line intensity relative to a Balmer line. Their argument is that the narrow H $\beta$  flux measurement is very uncertain, due to the difficulty of decomposing the narrow and broad components. This is true indeed. Notice however that some of the references regarding the observational data present the emission lines relative to H $\beta$ , without providing H $\beta$  absolute value (for example, Osterbrock & Koski 1976). In this case, A99 uses the absolute value from another data set. Furthermore, some of the references are extremely old, and clearly show serious problems with the measurements, mainly with the decomposition of the narrow and broad line components (for example, Oke & Sargent 1968 where H $\alpha$ /H $\beta$  = 1.61). Because of these problems, we decided to exclude data coming from references where H $\alpha$ /H $\beta$  is less than 2.8, since this clearly indicates a problem with the decomposition. In addition, as pointed out by A99, the narrow component of the UV lines (Kriss et al. 1992) show a FWHM which is 1.5 to 3 times larger than that of the NLR forbidden lines, which could also indicate a problem with the decomposition.

For NGC 1068, the absolute fluxes of the lines are provided by the authors in all references listed by A00. However, some measurements seemed to be problematic as well. Most of the observations were made in the 70's, with photographic plates. Some of the measurements are very discordant, which can be seen by the rms scatter in the A00 list. Taking this into account, we decided to use only the very strong optical and infrared lines, excluding problematic data from the average.

Therefore, averaged line intensities in our sample are not exactly the same as in A99 or A00. We choose to compare the observed and calculated line ratios, and not the absolute fluxes, adopting the line intensities relative to H $\beta$ . The line ratios corrected for reddening are presented in Table 1a and 1b, respectively, assuming E(B-V) = 0.03 for NGC 4151 and E(B-V) = 0.30 for NGC 1068, in agreement with those adopted by A99 and A00. In Tables 1a and 1b, the doublets are identified by the wavelength of one of the lines followed by a plus sign.



## 4. The Models

The photoionization code Aangaba (Gruenwald & Viegas 1992) is used to model the NLR of NGC 4151 and NGC 1068, assuming a plan-parallel symmetry. For each AGN, we first reproduce the results of the best fit given by A99 and A00, using the same input parameters, as listed in Table 2, where  $U$  is the ionization parameter,  $n$  the gas density,  $\epsilon$  the filling factor, and  $R_i$  the distance of the gas to the central source. Solar chemical abundances are adopted for modeling NGC 4151. On the other hand, for NGC 1068 a low oxygen abundance is assumed, as suggested by Netzer (1997) and adopted by A00 for their best fit model. From their models with a filling factor, A99 and A00 proposed that the continuum of these objects should be represented by a composition of power laws, as shown in Figures 3a and 3b, for NGC 4151 and NGC 1068, respectively. The continuum spectral shapes above  $10^3$  eV (X-rays) and below 10 eV (optical-UV) are obtained from observations, while between 10 and  $10^4$  eV several different shapes have been tested.

After reproducing the results of the best fit models proposed by A99 and A00 for NGC 4151 and NGC 1068, our next step is to explain the emission-line spectra using a multi-cloud model (based on single-cloud models with  $\epsilon = 1$ ), in order to test the spectral shapes suggested by A99 and A00, who excluded the presence of a blue bump.

### 4.1. NGC 4151 models

As claimed by A99, the spectrum showed by a solid line in Figure 3a (spectrum A) provides the best fit model for the observed narrow emission-lines of NGC 4151. Those authors did not find indications of a big blue bump in the ionizing continuum, which should appear beyond the Lyman limit. On the contrary, their best fit model suggests a trough in a power law.

As pointed out in §2, the trough in the ionizing spectrum could be an artifact which compensates for the systematic effect of a filling factor less than unity in the 1-D models. Thus, we look for multi-cloud models with another ionizing spectrum shape in order to verify if they are also able to reproduce the observed emission-lines.

For sake of comparison to a multi-cloud model, we reproduce the A99 best fit model using the code Aangaba with the input parameters listed in Table 2. Notice that our data set is slightly different from that used by A99, as explained above (§3), in particular the  $H\alpha/H\beta$  ratio, which is equal to 2 in their data set. In spite of the differences, the fitting to the data is as good as that presented by A99, as seen in Figure 4 where observed and calculated line ratios are confronted (to be compared with Fig. 8 of A99).

Models using other spectral shapes were also obtained. Among them, the model with spectrum B (Fig. 3a), showing a small blue bump, also provides a good fit to the observed lines, except for the high ionization lines, as expected from models with such type of continuum and assuming a filling factor less than unit. However, as in the case of the extragalactic HII region I Zw 18, we cannot exclude this kind of spectral shape, since the underestimation of the high ionization lines can also be due to  $\epsilon$  less than unit. In order to test this issue, multi-cloud models are also obtained. For this a grid of single-cloud models is built varying the density and the ionization parameter U.

The simplest composite model includes a low- and a high-density cloud, as adopted by Kraemer & Crenshaw (2000) in order to reproduce the the optical-UV emission-line spectrum of NGC 1068.

A grid of models for single-clouds characterized by the density ( $n$ ) and the ionization parameter (U) was obtained. The models were generated with these parameters in the range  $10^2\text{cm}^{-3} \leq n \leq 10^5\text{cm}^{-3}$  and  $0.005 \leq U \leq 4.0$ . To restrict the physical characteristics of the models we used the strong lines [OIII] $\lambda$ 5007+ and [MgVIII] $\lambda$  3.03  $\mu\text{m}$ . For a given value of U and varying the density, we look for the best two-density models which can explain these emission-lines. Once the densities are derived, we used all the observed emission-line intensities (Table 1a) to obtain the values of U for the low and high density clouds. The emission-line spectrum is reproduced by a four-cloud model. Notice that line ratios are not method dependent, i.e., the same cloud composition is found if we first define the values of U and then the cloud densities. The line ratios are obtained by a weighted average from the contributions from each of the four types of cloud. The ionization parameter, the gas density, and the H $\beta$  flux, as well as the fraction of H $\beta$  ( $g_i$ ) coming from each type of cloud, are listed in Table 3. This fraction is related to the area of the corresponding group of clouds photoionized by the central source. The largest contribution to the emission-line spectrum comes from the low-ionization, high density clouds.

A comparison between the observed and calculated emission-line ratios appears in Figure 5, where the results of A99 best fit are also plotted. It is easily seen that both the A99 model, using an ionizing SED with a trough and  $\epsilon < 1$ , and our four-cloud model, using an ionizing radiation SED with a bump (spectrum B) and  $\epsilon = 1$ , provide a similar fit to the observations. This can be verified by the  $\chi^2$  value, which are 2.27 and 2.28 respectively for the A99 best fit model and our multi-cloud model.

The multi-cloud model presented above is an example of the method used to fit the emission-lines and shows that the ionizing spectrum may show a bump instead of a trough as claimed by A99. In order to have a better determination of the ionizing continuum, additional constraints, coming from the observed continuum spectrum from radio to X-rays,

could be added to the model, as well as the contribution of an additional energy source, as discussed by Contini et al. (2002).

## 4.2. NGC 1068 models

In the case of NGC 1068, A00 do not find a single-component model that satisfactorily reproduces the observed emission lines. For this object, their best fit is a two-component model; one of the components is calculated with a radially varying filling factor. It is out of the scope of this paper to reproduce such a complex model for this object, since our goal is just to test the two approaches used to reproduce the emission-line spectrum of an inhomogeneous region with 1-D photoionization simulations. Therefore, we used input parameters of the best single-component model of A00 to discuss these two approaches, using the two shapes of the ionizing continuum plotted in Fig. 3b.

Spectrum A (Fig. 3b), with a trough, was assumed in the A00 single-cloud model which gives the best fit to the observations with the input parameters listed in Table 2. Spectrum B is an example of a bumpy continuum.

Following the procedure used for NGC 4151, the emission-line spectrum of NGC 1068 is first modeled using an uniform density distribution and a filling factor  $\epsilon < 1$ . The input parameters are listed in Table 2. The general conclusion is similar to the one obtained for NGC 4151, i.e., regardless of the spectral shape of the ionizing radiation, single-cloud models with  $\epsilon < 1$  overestimate the low ionization lines with respect to the high ionization lines, as already pointed out by A00. The comparison between observed and calculated emission-line intensities are shown in Figure 6 for both types of ionizing spectra.

We now look for the best fit multi-cloud model using the bumpy spectrum (spectrum B, Fig.3 ) in order to compare the results to those of A00 best fit model with ionizing spectrum A and  $\epsilon < 1$ . Following the same procedure adopted for NGC 4151 multi-cloud model, four types of clouds are defined. The characteristics of the single clouds, as well as the fraction of  $H\beta$  coming from each type of cloud, are presented in Table 4. The larger contribution to the total  $H\beta$  comes from the low-ionization low-density cloud.

The comparison between observed and calculated line ratios (Figure 7) shows that, except for the infrared lines  $[NeIII] 15.56$  and  $[NeIII] 36.01$ , our four-cloud fit, photoionized by a bumpy spectrum, is better than that provided by the best A00 single-cloud model. The corresponding  $\chi^2$  value for these models are 2.88 and 7.89, respectively.

Notice that A00 find that this simple filling factor model was not good enough to

reproduce the observed spectrum. They assumed a more complex two-component model, obtained from models with a filling factor. The low-density component has a constant filling factor, while the denser one a filling factor dependent on the distance. It is clear that our simpler multi-cloud model provides a very good fit to the observed line spectrum without the problems associated to and complexity required by their models with a filling factor.

## 5. Concluding Remarks

The emission-line spectra of the two well-known Seyfert galaxies NGC 4151 and NGC 1068 are used to test 1-D photoionization models for the NLR and to illustrate the misunderstanding introduced by the use of models with a filling factor less than unity to simulate inhomogeneous regions.

The ionizing radiation of AGN is not well known, but its shape, combined with the filling factor as it is introduced in 1- D photoionization codes, has a direct effect on the calculated emission lines. In the case of the extragalactic HII regions, for which the ionizing continuum is better known, we show that a multi-cloud model can explain all the observed features (size of the emitting region,  $H\beta$  luminosity and the significant emission-line ratios) without requiring an additional heating mechanism as inferred by SS99 who used models with  $\epsilon < 1$ .

Regarding the two Seyfert galaxies analyzed in this paper, we show that multi-cloud models are more appropriate to simulate the NLR. They provide a good fit to the observed emission-line spectra and do not exclude a bump in the SED of the ionizing radiation, as suggested by A99 and A00.

Two-component models have been used by Kraemer & Crenshaw (2000) to reproduce the optical-UV emission-line spectrum from several resolved zones of the NLR of NGC 1068. The hydrogen density of the dense components are in the range  $2.0 \times 10^4$  to  $2.5 \times 10^5 \text{ cm}^{-3}$  and the ionization parameter  $10^{-3.8} \leq U \leq 10^{-2.5}$ , while for the tenuous component the density varies from  $8.0 \times 10^2$  to  $2.3 \times 10^4 \text{ cm}^{-3}$  and  $10^{-2} \leq U \leq 10^{-1.6}$ . The values of the density and ionization parameters used in our multi-cloud model are in the range of those obtained for the two-cloud models proposed by Kraemer & Crenshaw for several resolved zones of the NLR of NGC 1068. Notice that our model simulates the whole NLR and also explains the infrared lines not included in Kraemer & Crenshaw discussion.

A more comprehensive multi-cloud model of the emission line spectrum of NGC 4151 is presented by Contini et al. (2002). The code used in the simulations includes the effect of shocks in the physical conditions of the emitting gas. The observed continuum data from

radio to X-rays are used to constrain the model and to find the contribution from the different clouds to the observed continuum and emission-line spectra. Noticed that the presence of shocks is also suggested by Kraemer & Crenshaw (2000).

In brief, in the last years the improvement of observational techniques, allowing observations with high spatial and spectral resolution, and providing a large amount of data in a wide range of wavelengths, has not been followed by a similar effort to improve the interpretation of the emitting regions with more realistic models. The standard 1-D photoionization models are becoming inappropriate to simulate emission-line regions like HII regions, planetary nebulae and active galactic nuclei. The new observations require more complex models regarding both additional mechanisms powering the emission (as shocks) and a better simulation of the geometry of the region with a more realistic gas distribution. It is clear that 3-D photoionization simulations would be more appropriate to analyze the NLR of AGN, as shown in the case of planetary nebulae (Gruenwald, Viegas & Broguière 1997, Monteiro et al. 2000). Such 3-D models will certainly contribute to a better discrimination of the possible nature of the ionizing radiation.

We are thankful to T. Alexander and H. Netzer for clarifying some of their results and data. We thank also Claus Leitherer for the careful reading of this paper. This paper is partially supported by FAPESP (00/06695-0, 00/122117-4) and CNPq (304077/77-1 and 306122/88-0), PRONEX/CNPq.

## REFERENCES

- Alexander, T., Sturm, E., Lutz, D., Sternberg, A., Netzer, H., Genzel, R. 1999, ApJ, 512, 204
- Alexander, T., Lutz, D., Sturm, E., Genzel, R., Sternberg, A., Netzer, H., 2000, ApJ, 536, 710
- Antonucci, R. 1993, ARA&A, 31, 473
- Antonucci, R. R. J., Miller, J. S. 1985, ApJ, 297, 621
- Axon, D. J., Marconi, A., Cappetti, A., Macchetto, F. D., Scherier, E., Robinson, A. 1998, ApJ, 496, L75
- Baldwin, J., Ferland, G., Korista, K. & Verner, D. 1995, ApJ 445L, 119
- Binette, L., Wilson, A. S. & Storchi-Bergmann, T. 1996, A&A 312, 365

- Cid-Fernandes, R., Dottori, H., Gruenwald, R. & Viegas, S. 1992, MNRAS, 255, 165
- Contini, M., Prieto, M. A. & Viegas, S. M. 1998a, ApJ 492, 511
- Contini, M., Prieto, M. A. & Viegas, S. M. 1998b, ApJ 505, 621
- Contini, M., Viegas, S. M., & Prieto, M. A. 2002, A&A, 386, 399
- Ferguson, J. W., Korista, K., Baldwin, J. & Ferland, G., 1997, ApJ 487, 122
- Gruenwald, R., Viegas, S. M. 1992, ApJS, 78, 153
- Gruenwald, R., Viegas, S. M., Broguiere, D. 1997, ApJ, 480, 283
- Izotov, Y. I., Thuan, T. X. 1998, ApJ, 497, 227
- Kaspi, S., Smith, S., Maoz, D., Netzer, H., Jannuzi, B. T. 1996, ApJ, 470, 336
- Kraemer, S. B. & Crenshaw, D. M. , ApJ, 551, 671
- Kriss, G. A., Davidsen, A. F., Blair, W. P., Bowers, C. W., Dixon, W. V., Durrance, S. T., Feldman, P. D., Ferguson, H. C. Henry, R. C., Kimble, R. A., Kruk, J. W., Long, K. S., Moos, H. W. & Vancura, O. 1992, ApJ, 392, 485
- Marconi, A., Van der Werf, P. P., Moorwood, A.F. M., Oliva, E. 1996, A&A, 315, 335
- Monteiro, H., Morrisset, C., Gruenwald, R., Viegas, S. M. 2000, ApJ, 537, 853
- Narayan, R., Kato, S., Homma, F. 1997, ApJ, 476, 49
- Netzer, H. 1997, Ap&SS, 248, 127
- Oke, J. B., Sargent, W. L. W. 1968, ApJ, 151, 807
- Oliva, E., Salvati, M., Moorwood, A. F. M., Marconi, A. 1994, A&A, 288,457
- Osterbrock, D. E. 1989, Astrophysics of Gaseous Nebulae and Active Galactic Nuclei, University Science Books (Mill Valley, California)
- Osterbrock, D. E. & Flatter, E. 1959, ApJ, 129, 26
- Osterbrock, D. E., Koski, A. T. 1976, MNRAS, 176, 61
- Penson, M. V., Perez, E. 1984, MNRAS, 211, 33
- Prieto, M. A. & Viegas, S. M. 2000, ApJ, 532, 238

- Rodriguez-Ardila, A., Viegas, S. M., Pastoriza, M. G., Prato, L. 2002, ApJ, 565, 140
- Schulz, H., Komossa, S. 1993, A&A, 278, 29
- Stasinska, G. & Schaerer, D. 1999, A&A, 351,72
- Terashima, Y., Iyomoto, N. , Ho, L. C., & Ptak, A. F. 2002, ApJS, 139, 1
- Viegas, S. M. 2002, Rev. Mex. (Conf. Ser.), 12, 219
- Viegas, S. M., Contini. M. & Contini, T. 1999, A&A, 317,112
- Viegas-Aldrovandi, S. M., Gruenwald, R. 1988, ApJ, 324, 583
- Wilson, A.S., Ulvestad, J. S. 1983, ApJ, 275, 8

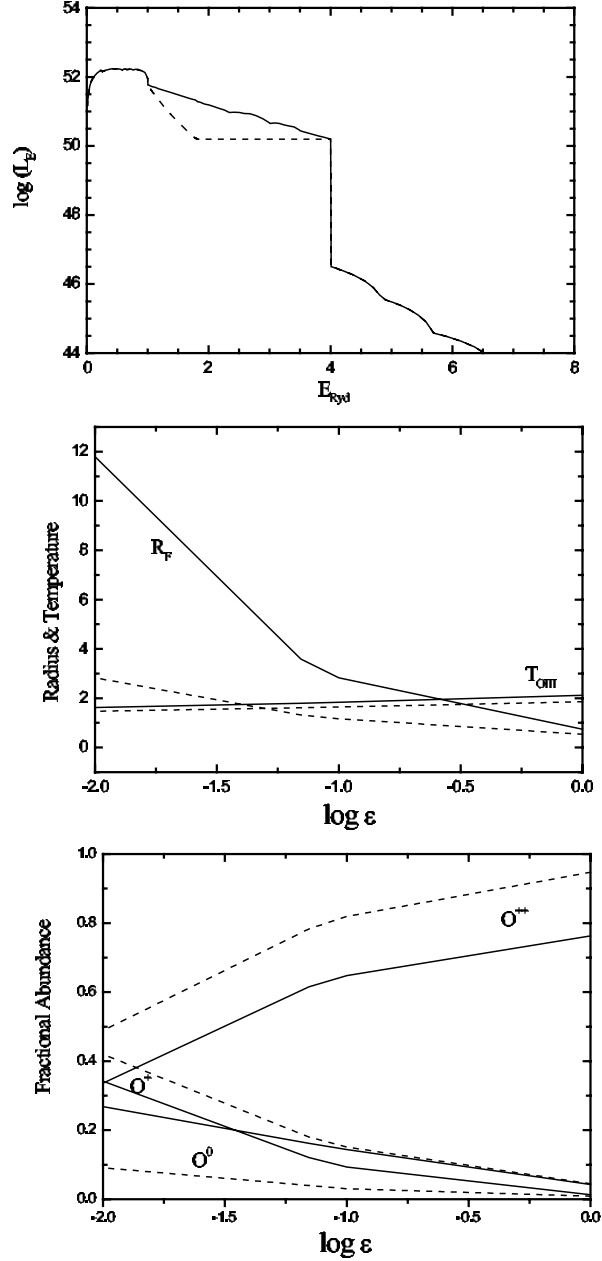


Fig. 1.— The effect of the filling factor on 1-D models. Top-panel: The zero-age stellar cluster ionizing spectrum (solid line) and a modified spectrum, with less photons above the Lyman limit (dashed line). Middle-panel: the radius of the ionized region ( $R_F/10^{20}\text{cm}^{-2}$ ) and the average temperature ( $T_{OIII}/10^4\text{K}$ ) as a function of the filling factor. Bottom-panel: the ionization fraction of  $O^0$ ,  $O^+$  and  $O^{++}$  as a function of the filling factor. The solid lines correspond to the results of models with the zero-age stellar cluster spectrum and the dashed lines to those obtained with the modified spectrum.



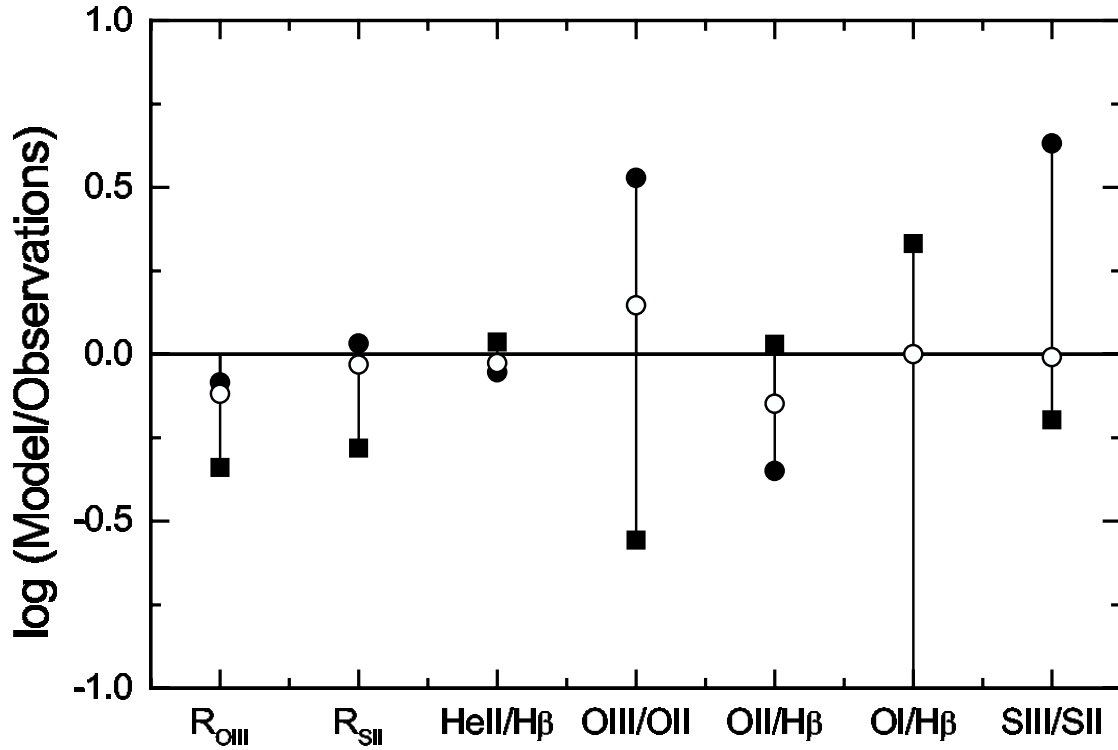


Fig. 2.— Comparison of calculated and observed emission-line ratios for IZw 18. The results correspond to a homogeneous model (filled circle), a condensation (filled square) and a composite model (open circle) for which 60% of the  $\text{H}\beta$  emission comes from the dilute homogeneous gas distribution ( $30 \text{ cm}^{-3}$ ) and 40 % from the condensation ( $10^4 \text{ cm}^{-3}$ ).

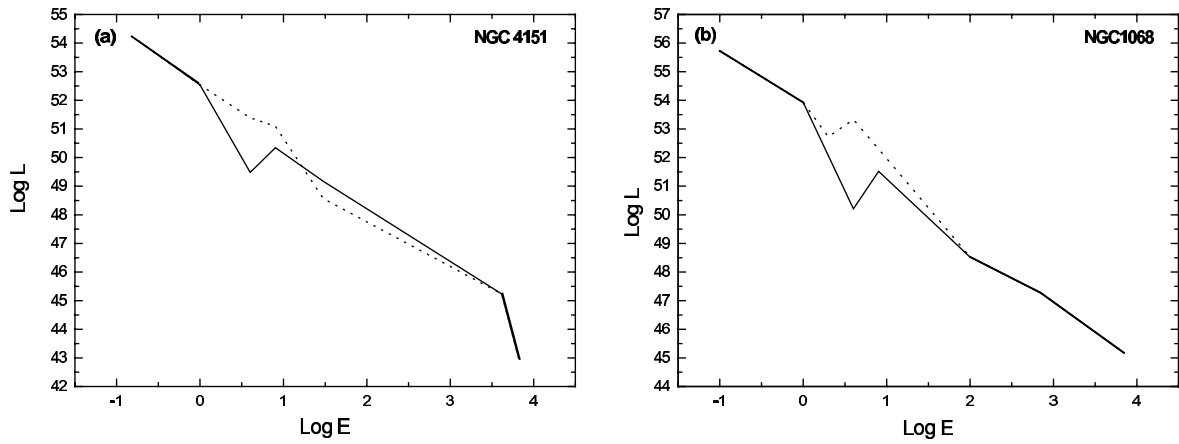


Fig. 3.— (a) Ionizing radiation spectrum for NGC 4151. The spectral luminosity is given in units of photons  $s^{-1} eV^{-1}$  and the energy in Ryd. The thick solid line corresponds to observations, the thin solid line to the spectral shape A used in the best fit model of A99, while the dotted line represents a bumpy shape B (see text). (b) Ionizing radiation spectrum for NGC 1068. The notation is the same as in Figure 2a.

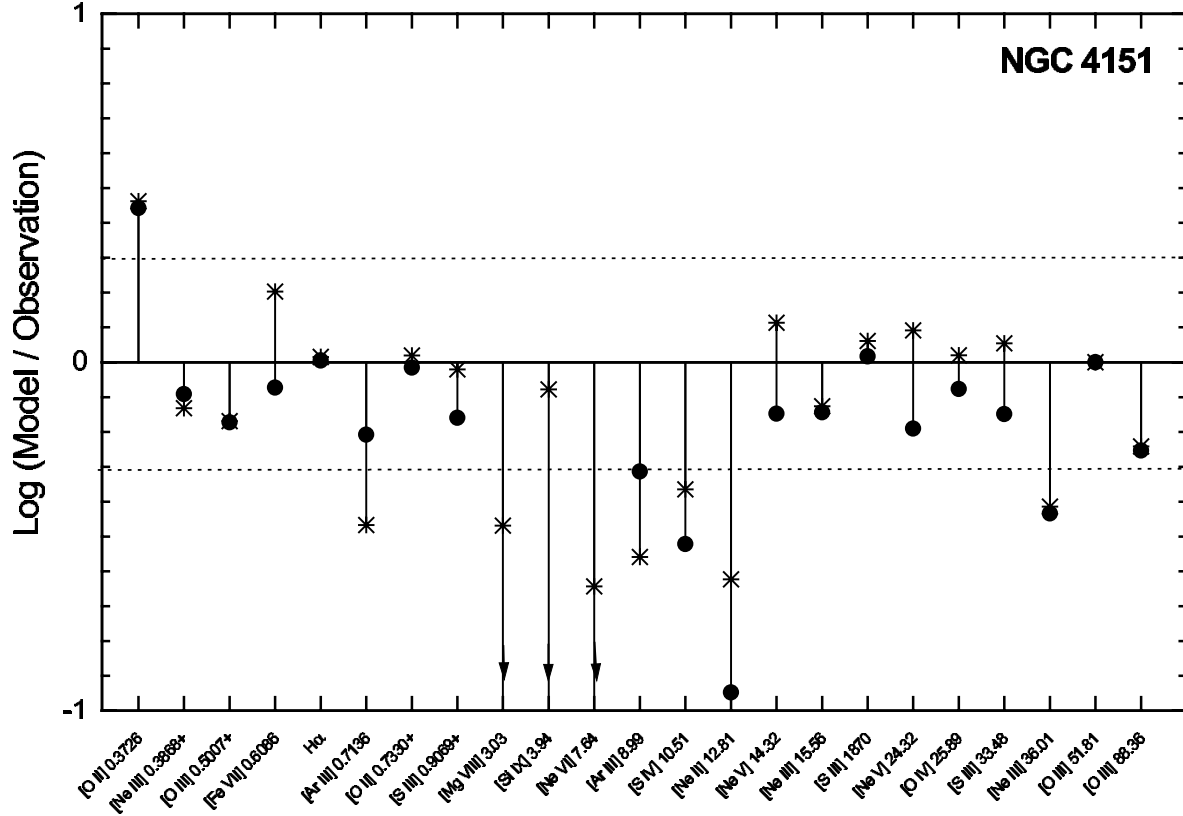


Fig. 4.— Comparison of calculated and observed emission-line ratios for NGC 4151. The results correspond to the single-cloud models using a filling factor  $\epsilon = 0.025$  with spectrum A (star) and spectrum B (filled circle). The SED of the ionizing radiation are shown in Fig 2a. The emission-lines are identified only by the ion in the horizontal axis following the order of wavelengths as in Table 1a.

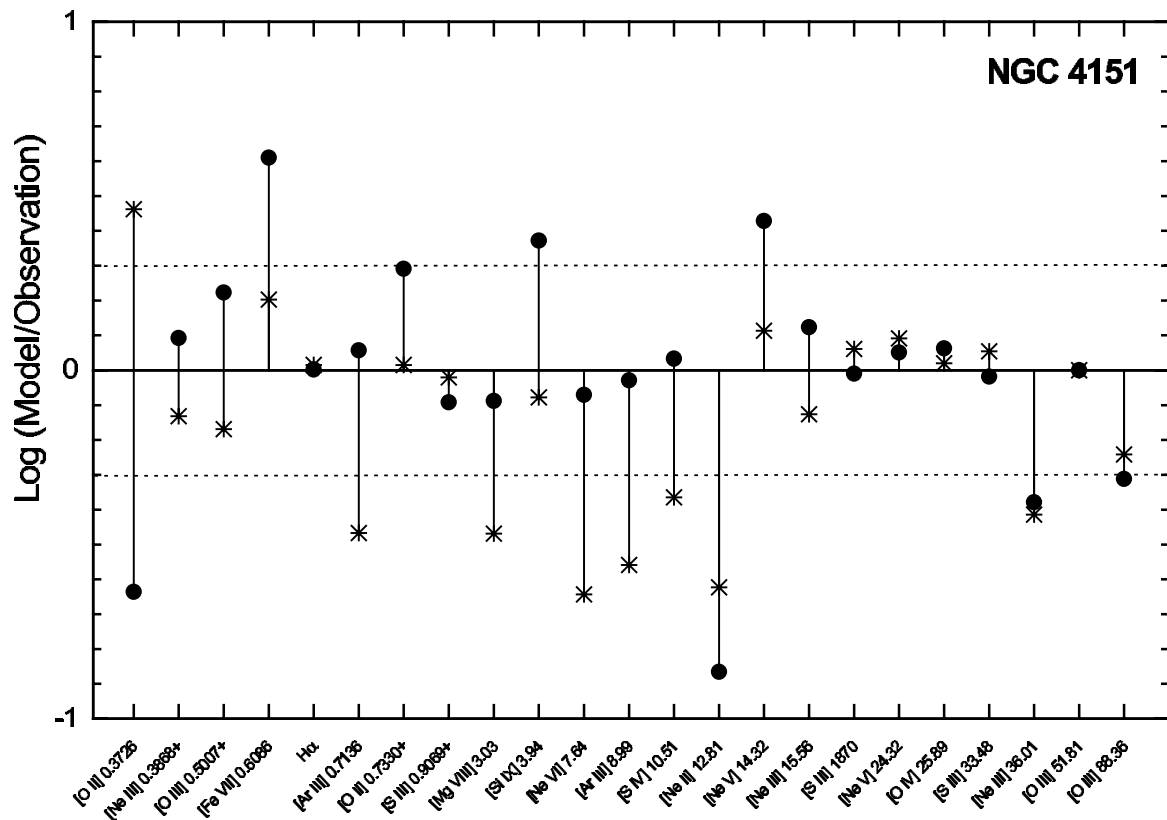


Fig. 5.— Comparison of calculated and observed emission-line ratios for NGC 4151. The results correspond to the single-cloud model using a filling factor  $\epsilon = 0.025$  with spectrum A (star) and the multi-cloud model using spectrum B (filled circle). The SED of the ionizing radiation is shown in Fig 2a. The emission-lines are identified only by the ion in the horizontal axis following the order of wavelengths as in Table 1a.

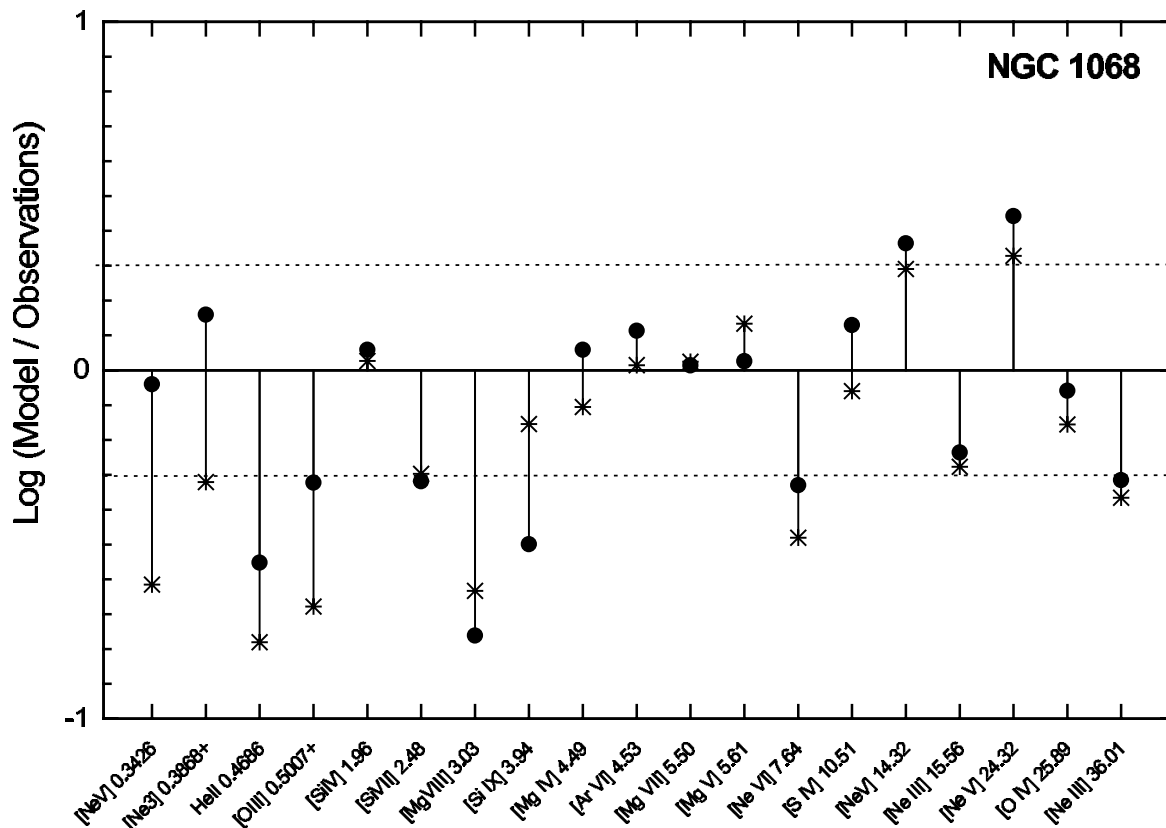


Fig. 6.— Comparison of calculated and observed emission-line ratios for NGC 1086. The results correspond to the single-cloud models using a filling factor  $\epsilon = 0.1$  with spectrum A (star) and spectrum B (filedcircle). The SED of the ionizing radiation are shown in Fig 2b. The emission-lines are identified only by the ion in the horizontal axis following the order of wavelengths as in Table 1b.

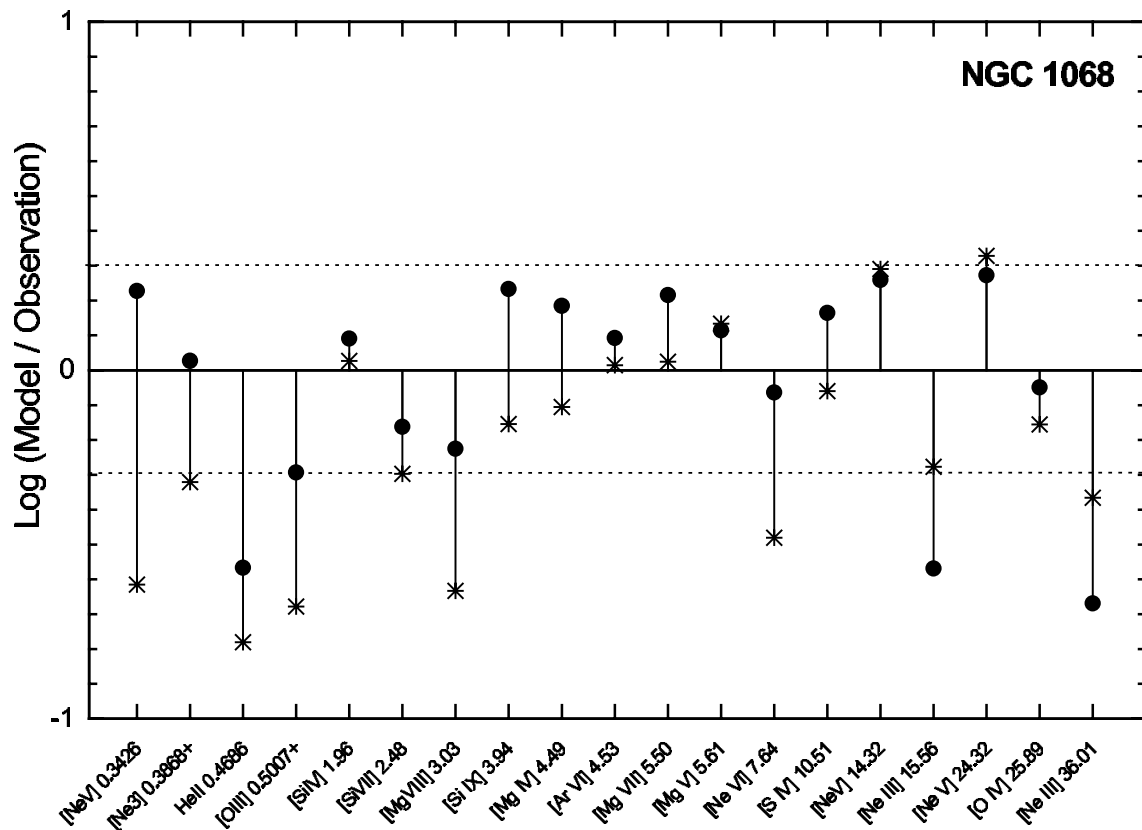


Fig. 7.— Comparison of calculated and observed emission-line ratios for NGC 1068. The results correspond to the single-cloud model using a fillingfactor  $\epsilon = 0.1$  with spectrum A (star) and the multi-cloud model using spectrum B (filled circle). The SED of the ionizing radiation are shown in Fig 2b. The emission-lines are identified only by the ion in the horizontal axis following the order of wavelengths as in Table 1b.

Table 1. a NGC 4151 observed emission-lines

Line ( $\mu\text{m}$ )	$\mathbf{I}_\lambda/\mathbf{I}_{H\beta}$
[O II]0.3726+	2.968
[Ne III]0.3868+	2.196
[O III]0.5007+	13.287
[Fe VII]0.6086	0.113
H I 0.6563	2.869
[Ar III]0.7136	0.194
[O II]0.7330+	0.257
[S III]0.9069+	1.958
[Mg VIII]3.03	0.032
[Si IX]3.94	0.021
[Ne VI]7.64	0.371
[Ar III]8.99	0.103
[S IV]10.51	0.522
[Ne II]12.81	0.541
[Ne V]14.32	0.251
[Ne III]15.56	0.943
[S III]18.70	0.245
[Ne V]24.32	0.253
[O IV]25.89	0.914
[S III]33.48	0.363
[Ne III]36.01	0.157
[O III]51.81	0.460
[O III]88.36	0.302

Table 1. b NGC 1068 observed emission-lines

<b>Line (<math>\mu\text{m}</math>)</b>	<b><math>\mathbf{I}_\lambda/\mathbf{I}_{H\beta}</math></b>
[Ne V]0.3426	1.521
[Ne III]0.3868+	1.632
He II 0.4686	0.381
[O III]0.5007+	15.397
[Si IV]1.96	0.170
[Si VII]2.48	0.175
[Mg VIII]3.03	0.221
[Si IX]3.94	0.096
[Mg IV]4.49	0.142
[Ar VI]4.53	0.280
[Mg VII]5.50	0.237
[Mg V]5.61	0.327
[Ne VI]7.64	1.935
[S IV]10.51	0.996
[Ne V]14.32	1.637
[Ne III]15.56	2.690
[Ne V]24.32	1.159
[O IV]25.89	3.140
[Ne III]36.01	0.279



Table 2. Input parameters

	NGC 4151	NGC 1068
U.....	0.025	0.1
n.....	$10^3 \text{ cm}^{-3}$	$2 \times 10^3 \text{ cm}^{-3}$
$\epsilon$ .....	$6.5 \times 10^{-4}$	$1 \times 10^{-3}$
$R_i$ .....	$1.46 \times 10^{20} \text{ cm}$	$1.82 \times 10^{20} \text{ cm}$

Table 3. NGC 4151 multi-cloud model

$\mathbf{U}$	$\mathbf{n}$ $\text{cm}^{-3}$	$\mathbf{F}_{H\beta}$ $10^7 \text{ ergs/cm}^2/\text{s}$	$\mathbf{g}_i$
0.005	$10^3$	.002	0.082
0.005	$10^5$	1.90	0.869
0.4	$10^3$	1.46	0.028
0.2	$10^5$	147.	0.021

Table 4. NGC 1068 multi-cloud model

$\mathbf{U}$	$\mathbf{n}$ $\text{cm}^{-3}$	$\mathbf{F}_{H\beta}$ $\text{ergs/cm}^2/\text{s}$	$\mathbf{g}_i$
0.005	$10^3$	.043	0.549
0.1	$10^4$	.118	0.237
0.1	$10^3$	1.16	0.008
0.01	$10^5$	10.3	0.207